IEEE Access
Multidisciplinary ⋮ Rapid Review ⋮ Open Access Journal

Received 10 June 2023, accepted 25 June 2023, date of publication 28 June 2023, date of current version 6 July 2023.

Digital Object Identifier 10.1109/ACCESS.2023.3290496

RESEARCH ARTICLE

DeepDDM: A Compact Deep-Learning Assisted Platform for Micro-Rheological Assessment of Micro-Volume Fluids

UNGKARN JARUJAREET[1], KANNIKA WIRATCHAWA[2], PIYAPHONG PANPISUT[3,4], AND THANAPONG INTHARAH[2]

[1]NECTEC, National Science and Technology Development Agency (NSTDA), Khlong Luang, Pathum Thani 12120, Thailand
[2]Visual Intelligence Laboratory, Department of Statistics, Faculty of Science, Khon Kaen University, Khon Kaen 40002, Thailand
[3]Faculty of Dentistry, Thammasat University, Khlong Luang, Pathum Thani 12120, Thailand
[4]Thammasat University Research Unit in Dental and Bone Substitute Biomaterials, Thammasat University, Khlong Luang, Pathum Thani 12120, Thailand

Corresponding author: Thanapong Intharah (thanin@kku.ac.th)

This work was supported by the National Science, Research and Innovation Fund (NSRF) via the Program Management Unit for Human Resources and Institutional Development, Research and Innovation, under Grant B05F650016.

ABSTRACT An emerging differential dynamic microscopy technique has been successfully used for quantitative dynamic investigation of micro-particle suspension, leading to a rheological assessment of the solution. This technique exploits an optical microscope equipped with a digital camera for the assessment. However, the accessible measurement ranges at high frequencies are limited by the video frame rate of the camera, resulting in a limitation in investigating distinguish responses at the high-frequency region. With advanced deep learning technology, image-synthesizing deep learning-based algorithms can significantly increase the video frame rate, producing additional in-between frames. As a result, the rheological responses at the high-frequency region can be obtained. To address this problem, a video frame interpolation integrated differential dynamic microscopy-based device (DeepDDM platform) was developed. Our DeepDDM platform interpolates video frames to extend the maximum measuring angular frequency up to quadruple from 30.1 rad/s to 123.0 rad/s, resulting in a more comprehensive rheological assessment without hardware modification. Unlike reducing the camera exposure time approach, our approach requires only a single camera and works without brightness reduction. Furthermore, the device is compact and portable. It comprises a few main components, and requires only 8 μL sample volumes for the rheological assessment. Thus, it is easy to relocate to measure biological samples which are often do not retain their natural properties in a storage allowing for in situ studies of the fluids. In comparison, the obtained responses agreed with the reference mechanical rheometer, although the employed partially coherent source and out-of-focus image acquisition bring difficulties to our system.

INDEX TERMS Differential dynamic microscopy, rheology, deep learning, frame interpolation.

I. INTRODUCTION

Rheological characterization is essential for bio-fluid understanding, design, and development. This is because bio-fluids are often complex as they may consist of many intrinsic micro-structures [1]. These micro-structures influence the materials' flow behavior, which can be investigated using rheology [1], [2], [3]. For example, the natural physical behavior of human saliva is primarily composed of water exhibiting more than 99.0% and several minor components such as glycoproteins and enzymes [4], [5], [6]. According to many studies, the whole human saliva behaves like a shear thinning fluid [7], [8], [9] with regardless of the collection method [10]. This lubricious nature of saliva is a crucial behavior promoting speech and swallowing of a food bolus [8]. It also maintains oral health protecting the mucosa

The associate editor coordinating the review of this manuscript and approving it for publication was Jiafeng Xie.

from bacterial attack, fungal growth, and demineralization of teeth [8], [11], [12], [13]. In human blood plasma, water also primarily accounts for more than 90.0% while the rest are a mixture of proteins, coagulants, electrolytes, and immunoglobulins [14]. Although plasma and saliva are composed of a considerable amount of water with more than 90% of its content, plasma behaves as opposed to saliva. It is considered as a Newtonian fluid whose viscosity does not depend on an applied shear [15], [16]. Therefore, rheological characterization of the materials is essential for understanding the material behavior to precisely control their properties for delivering a specified mechanical response.

In a conventional approach, a mechanical rheometer usually examines a fluid's rheological properties. For example, a stress-controlled rheometer imposes constant torque using rotating cylinders, cones, or plates to determine the rheological responses of the test fluid. However, this approach requires milliliter sample volumes for a measurement to obtain a reliable result [17]. Unfortunately, some emerging biological fluids are hard to synthesize or impossible to obtain in large quantities [2], [18], [19]. Thus, the rheological characterization of these fluids is considerably expensive. In addition, many soft materials exhibit a weak modulus [2], [20] leading to an inconsistency resulting in this approach as deviations in rotational symmetry and overfill/underfill samples allow surface tension to produce torque at a low shear rate [21].

Investigating the light scattering phenomenon from a material is a promising approach for many applications ranging from research to industry. For example, light scattering was used to monitor product development and quality control in the pharmaceutical industry [22], [23]. In biomedical applications, a light scattering technique successfully determined the enzyme activity in an enzyme assay [24], [25], [26]. Light scattering can also be used as a tool to design new polymeric material with a tiny sample volume requirement [27]. Among light scattering approaches, dynamic light scattering (DLS) is one of the most widely used light scattering techniques [2] as it is a powerful, fast, and non-invasive analytical tool for the characterization of macromolecules and nanoparticles in a solution [28], [29].

In a typical configuration, a DLS instrument measures the temporal fluctuations of the scattered light due to the hydrodynamic motions of particles in the solution. By analyzing these fluctuations, the translational diffusion coefficient of the particles can be determined. Despite particle characterization, the generalized Stokes-Einstein relation (GSER) development allows for rheological assessment of a solution using the standard DLS instrument [2], [30], [31] as it relates the motion of the particles to infer the viscoelastic modulus assessment of the solution.

Unlike the DLS, differential dynamic microscopy (DDM) is an emerging approach to performing light scattering experiments. The DDM is based on using a standard optical microscope to retrieve particle dynamic information that is equivalent to a DLS [32]. In the DDM experiment, a time series of images is acquired by the microscope camera [32]. Fourier analysis of the difference between images in the series is calculated and separated by a given lag time τ, resulting in intensity fluctuations to decay as a function of wavevector q. This result allows for characterizing the dynamics of the employed particles in a fluid of interest. DDM offers many advantages over DLS [33]. For instance, it is a simple configuration and can measure the region of interest. It is also invariant to undesirable static stray-light contributions caused by dust and scratches in its optical path. However, the DLS is sensitive to them, particularly at low scattering angles [34], [35].

The DDM uses the passive microrheology principle, in which the motion of embedded tracer particles is monitored and recorded. For example, a DDM device was realized as a tool for the rheological characterization of sucrose and worm-like micelle solutions, including polyacrylamide gels [36]. By retrieving the mean square displacement ($\Delta r^2(\tau)$) of employed gold nanoparticles in such samples. The viscoelastic modulus ($G^*(\omega)$) can be obtained using the GSER [30], [31] as $G^*(\omega) = \frac{2K_BT}{3\pi ai\omega\mathcal{F}(\Delta r^2(\tau))}$, where K_BT is Boltzmann constant, T represents temperature, a is the radius of the particle,$\mathcal{F}$ is the Fourier operator, and ω is the angular frequency. The modulus is a of viscoelastic material describing how viscous and elastic the material is.

High frequency rheometry are defined as measurement in the frequency range beyond that accessible by conventional rotational rheometry (f > 100 Hz) [37], [38] which is limited by mechanical limitations and inertial effects in the gap loading limit [38]. Nevertheless, investigating materials in a high-frequency region reveals rheological properties that differ from those in a low-frequency region [39]. In an entangled solution of wormlike micelles, exploring the high-frequency region is expected to unveil the mesh size of the micelles network [40]. High-frequency rheology also provides an advantage for investigating surface properties [41]. Thus, the high-frequency extension allows for a more comprehensive rheological characterization benefiting a particular bio-fluid design [42] and study.

Nevertheless, the accessible frequency ranges of the DDM are limited by the acquisition frame rate of the employed digital video camera [32]. The highest accessible frequency can be determined by the inverse of the maximum acquisition frame rate of the camera [43], [44]. As a result, investigating the dynamics faster than the camera acquisition frame rate is impossible. An extension to the DDM was proposed to address this limitation [43]. This device illuminated the sample with pulses of blue and red light-emitting diodes and recorded the image. Subsequently, the blue and red image channels of the image were decomposed from a single RGB image, allowing for the investigation of dynamical changes with a much smaller time scale than the exposure time of the image. Although the result agrees with those obtained using

a typical DDM setup, this approach produced more variation. In cross-correlation DDM [44], a dual-camera microscope was used for quantifying the fast dynamics of a nematic liquid crystal. Cross-correlation analysis of images acquired by two randomly triggered cameras. However, time synchronization between the external triggers and their associated cameras must be accurate enough to reduce memory consumption resulting in real-time processing [44].

To achieve a compact DDM platform that can instantly measure rheological properties at the sample collection site yet with a more comprehensive rheological characterization compared to the standard DDM, we proposed DeepDDM, a compact platform of a video frame interpolation integrated DDM-based device to address this problem using a Convolutional Neural Network (CNN) interpolation [45], [46]. Unlike reducing camera exposure time, our approach interpolated in-between frames to increase the recorded video's frame rate without reducing the brightness resulting in access of rheological properties at higher angular frequency. We also demonstrated a rheological assessment of fluid of interests that can be accessed at a frequency beyond the camera frame rate. We showed our device produced a more comprehensive assessment of fluid properties of interest, surpassing the capabilities of the standard DDM method, all without the need for an external trigger.

This paper was organized as follows. In Section II, material and methods used for rheological analysis were provided. Experimental results of the reference materials and artificial saliva were also demonstrated and presented in Section III. Discussions and conclusion of the main findings were provided in Section IV and V, respectively.

II. MATERIAL AND METHODS

In this section, sample preparation and the method used for measuring the rheological properties of the samples were provided. For our device, the measurements were performed at a controlled room temperature of 25°C. In measurement, a tiny amount of tracer particle solution was added to a test sample to probe their motions. Then, approximately 8.0 μL of the mixture was pipetted and dispensed in a microchamber with a nail varnish seal on its edges to prevent sample evaporation. Following this, the device recorded a series of images of a sample. Then, video frame interpolation algorithms were applied to the recorded images synthesizing new in-between images of the series. Subsequently, a mechanical rheometer (ARES G2, TA Instruments Inc.) was used as a reference in validation.

A. SAMPLES PREPARATION

A simple validation of the measured rheological properties of our device was carried out by measuring well-characterized fluids, i.e., water and glycerol-water mixtures. These samples were prepared and measured using our device and verified by the rheometer and the published data [47]. For an artificial saliva sample, the rheometer was used for verification.

TABLE 1. Chemicals used for preparing an artificial saliva.

Chemicals[1]	Amount(g)
Methl-p-hydroxybenzoate	2.00
Sodium carboxymethyl cellulose	10.00
$MgCl.6H_2O$	0.06
$CaCl_2$	0.13
K_2HPO_4	0.80
$K_2H_2PO_4$	0.33
KCL	0.63

1) TRACER PARTICLES SOLUTION

An initial concentration of 1.0 μm polystyrene microparticles (07310-15, Polysciences Inc.) was diluted in deionized water ten times and kept in an Eppendorf tube, and it was gently shaken before use.

2) DEIONIZED WATER

A deionized water sample was prepared by adding a 1.0 μL of the tracer particles solution to 200.0 μL of deionized water. However, approximately 8 μL was pipetted and dispensed in a microchamber for measurement.

3) GLYCEROL-WATER MIXTURES

Aqueous-glycerol mixtures were prepared by dissolving glycerol into deionized water at percentages by weight (%wt) of 20, 40, and 60. Then, a small amount of the tracer solution was added to these mixtures at a mixing ratio of 1:200 prior to measurement.

4) ARTIFICIAL SALIVA

An artificial saliva used in this research was prepared according to the Table 1. These organic and inorganic chemicals were weighted using a four-figure balance, mixed, and gradually added a total of 1000 mL of deinoized water. The artificial saliva solution were adjusted its PH values to 6.75 form adding a small amount of KOH (Sigma-Aldrich, St. Louis, Missouri, USA).

B. BULK RHEOMETRY

A mechanical rheometer (ARES G2, TA Instruments Inc.) in a 50 mm parallel plate geometry was used as a reference rheological measurement. The gap size between the plates was set at 0.5 mm. During a measurement, a solvent trap was always used to prevent sample evaporation. Approximately 1 mL of sample was used for determining its rheological responses, with the sample temperature being controlled at 25°C.

C. A COMPACT DIFFERENTIAL DYNAMIC MICROSCOPY-BASED DEVICE

In the compact differential dynamic microscopy, a monochromatic light-emitting diode (LED) was coupled with an optical fiber end in our light illumination, while the other end was coupled with a collimator creating a parallel light. Following this, the light travels through a sample accommodated in a

sample container. An objective lens enlarged the light, then recorded at 30 fps by the imaging sensor of the device at a controlled room temperature of 25°C. In measurement, our device collected a time series of 4,000 images and cropped these images to the predefined size of 800 × 800 pixels from their centers. Color-to-grey image transformation was applied to the images prior to the DDM analysis. The schematic and our device assembly are shown in Fig. 1.

In the differential dynamic algorithm (DDA), dynamic scattering patterns can be recovered from the analysis of ensemble dynamics of complex fluids [32]. This can be done by determining intensity alteration between two images separated by a lag time τ. The Fourier transform of the difference image $\Delta I(q, \tau)$ was calculated, then, computed its Fourier power spectrum as $S(q, \tau) = \langle |\Delta I(q, \tau)|^2 \rangle$, where $S(q, \tau)$ being image structure function, q is a wavevector, and τ represents a lag time. The image structure function can be modelled as follows: [32], [36], [48], [49].

$S(q, \tau) = A(q)(1 - f(q, \tau)) + B(q)$, where the amplitude $A(q)$ is related to the scattering properties of the particles and the optical transfer function of the imaging optics [32], [36], [48], [49], $B(q)$ is a noise term, and f is the normalized intermediate structuring function.

As aforementioned, the mean square displacement ($\langle \Delta r^2(\tau) \rangle$) of employed tracer particles can infer the rheological properties of a test fluid. This measure indicates how much the particles move over a given time interval. Having tracer particles employed, this statistical motion can be related to the normalized intermediate structuring function f with $f = e^{\frac{q^2 \langle \Delta r^2(\tau) \rangle}{4}}$ and can be obtained by $\langle \Delta r^2(\tau) \rangle = \frac{4}{q^2} ln \left(1 - \frac{S(q,\tau) - B(q)}{A(q)}\right)$ [36], [50].

Once ($\langle \Delta r^2(\tau) \rangle$) is obtained, the viscoelastic modulus $G^*(\omega)$ can be estimated by the GSER [30], [31], [36], [51]. Then, the complex viscosity is obtained from the modulus. However, the modulus of the complex viscosity is used as a measure for estimating steady-shear viscosity according to the empirical Cox-Merz relationship [50] as $|\eta^*(\omega)|_{\omega \to 0} \equiv \eta(\dot{\gamma})_{\dot{\gamma} \to 0}$.

D. OUR DeepDDM PLATFORM

Our DeepDDM platform consisted of the previously mentioned compact DDM (see, Sec.II-C), the DDA, and a video frame interpolation algorithm. The DeepDDM collects a series of images separated by a lag time τ. Then, a video frame interpolation interpolates in-between images of the image series resulting in a new image series of n+(n-1) images, where n is the total number of images in the original series. However, the total recording time of these additional synthesized images is unchanged by this procedure, causing a double in the original frame rate. The DDA is applied to the new image series and the original image series yielding two image structure functions. Then, these two structure functions are merged by scaling their time scales to be matched according to the procedure detailed in the literature [52]. To investigate the rheological property of a fluid of interest, the mean square displacement of the embedded micro-particles is obtained from the merged structure function, as previously mentioned. Once the mean square displacement is obtained, the visco-elastic modulus ($G^*(\omega)$) of the fluid can be determined using the GSER. To obtain the complex viscosity ($\eta^*(\omega)$) of the fluid, the visco-elastic modulus is calculated using $\eta(\omega) = G^*(\omega)/i\omega$, where i being an imaginary number, and ω is the frequency of deformation. The overall workflow of our DeepDDM can be summarized as shown in Fig. 2.

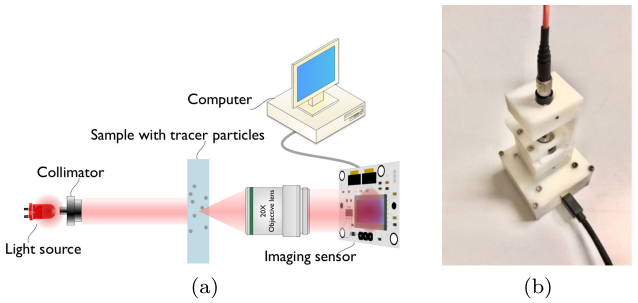

FIGURE 1. Our developed device consisted of a light source, an objective lens, and a camera shown in (a) and (b) was the device assembly.

1) VIDEO FRAME INTERPOLATION

Hardware systems are subject to inherent limitations due to the nature of their constituent parts and components. Our proposed DDM device also reached the constraint of the image sensor, which limited the frame rate; therefore, the measurement range of the device is limited by the camera limitation. To extend the measurement range of the device so that it can measure a higher shear rate, we choose to increase the frame rate algorithmically.

In this work, we boost the number of frame rates using a frame interpolation algorithm. The goal of frame interpolation is synthesizing intermediate images between pairs of input images. As our DDM aims to observe particle motion, consecutive frames are considered near duplicates. We pick a Convolutional Neural Network (CNN) based interpolation algorithm based over conventional optical flow-based interpolation algorithms [45], [46] due to the latter needed accurate optical flow estimation, which is challenging to obtain. We use the trained Frame Interpolation for Large Motion network [53] to do image interpolation as the network generalizes well on both small and large motions.

FILM uses the bi-directional motion estimation module that works independently of the scale based on a multi-scale feature extractor that shares weights across the scales. The approach relies on the intuition that large motion at finer scales is similar to small motion at coarser scales. The network is composed of three stages: the scale-agnostic feature extraction stage, the flow estimation stage, and the fusion stage. The feature extraction stage uses scale agnostic feature pyramid extraction. The flow estimation stage then uses a feature from the first stage to compute a bi-directional

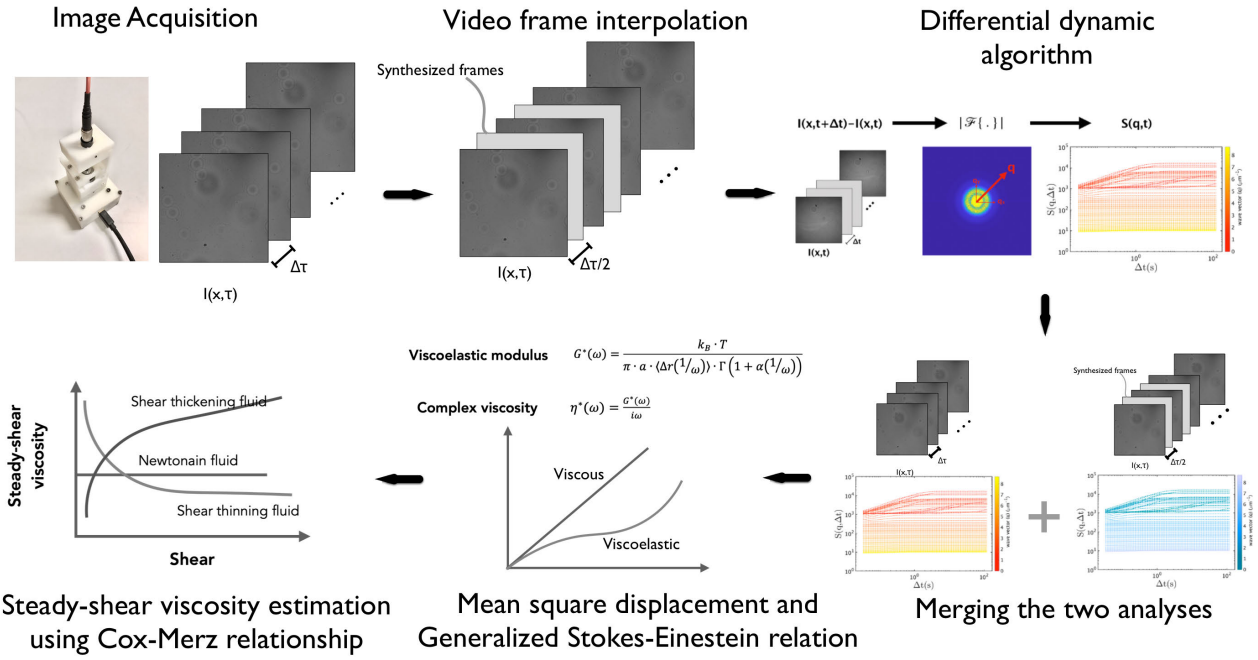

FIGURE 2. **Overall workflow of our DeepDDM device.**

motion at each pyramid level. Finally, the fusion stage used UNet-like decoder to synthesize the interpolated frame from the scale agnostic feature maps and the bi-directional motions from different pyramid levels.

We increase the frame rate of the particle moving video from the DDM by synthesizing interpolated images for multiple generations. Each generation doubles the angular frequency of the device. We use two consecutive frames of the current generation, raw images from the image sensor are considered as *generation 0*, and the input generates the interpolated frame between the two. *Generation G* composed of frames from *generation G-1* and the interpolated frames. We synthesize the interpolated frames between all frames from the current generation, which makes $n + (n - 1)$ frames for the *generation G* where n is the number of frames of *generation G-1*. We experimented with the frame interpolation with four generations, as shown in Fig 3.

For the trained FILM network used in the DDM, we used the original implementation from the author, which is based on the TensorFlow library. The network was pre-trained on the Vimeo90K dataset [54]. After the fourth generation, all frames are processed with the DDA.

III. EXPERIMENTAL RESULTS

A. VALIDATION OF THE COMPACT DIFFERENTIAL DYNAMIC MICROSCOPY

Validation of the compact DDM is essential to ensure that our DeepDDM produces a reliable result because the DeepDDM was developed based on compact DDM with an additional video frame interpolation algorithm. The validation measured how much viscosity measurement deviated from the published value, including the measurement obtained from a commercial mechanical rheometer (ARES G2, TA Instruments Inc.). In this experiment, well-defined fluids, such as deionized water and glycerol-water mixtures, were investigated and compared to the published data and the reference mechanical rheometer.

1) DEIONIZED WATER

To measure the rheological properties, a volume of the tracer solution was added to the water at a mixing ratio of 1:200. A sample volume of approximately 8.0 μL was dispensed in a microchamber and placed in the sample holder of our device. Then, 4,000 images were collected from the device. The DDA analyzed these images to retrieve the mean square displacement of the employed tracer particles. The GSER was applied to the mean square displacement yielding loss and storage moduli of the water. Accordingly, the modulus of the complex viscosity of the water was calculated from the obtained loss and storage moduli shown in Fig. 4.

From Fig. 4, the modulus of complex viscosity of the water was three-fold replicated to obtain the mean and standard deviation of the measurement. Then, the obtained modulus was averaged across all angular frequencies to compare with the reference value [47]. In analogy to the reference value, the averaged value was at $0.92 \pm 0.03\ mPa \cdot s$ with the percentage absolute error of 1.0%.

2) GLYCEROL-WATER MIXTURES

The varying viscosity of a measuring fluid allows for determining the accessible viscosity ranges of the developed

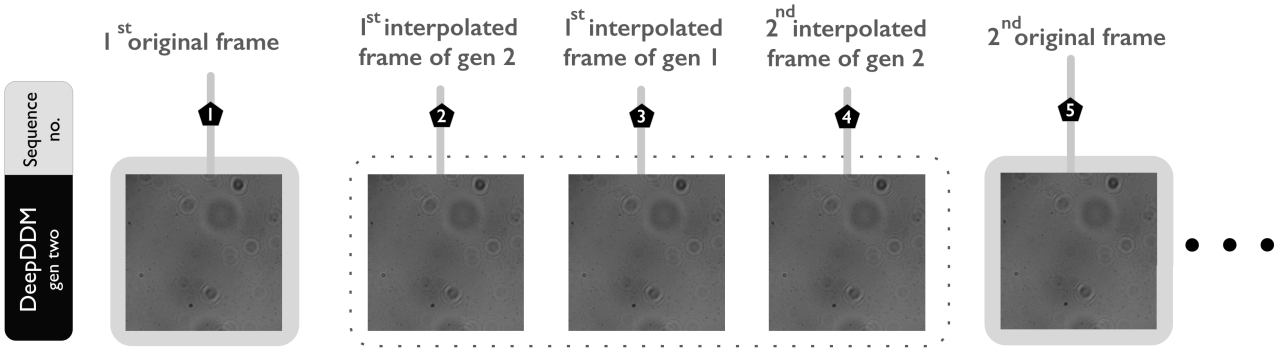

FIGURE 3. A DeepDDM for generation two of an artificial saliva sample.

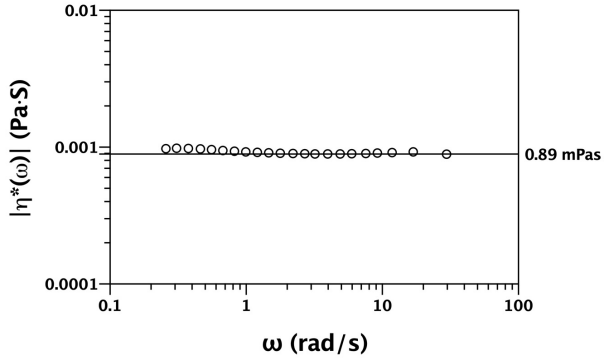

FIGURE 4. The modulus of complex viscosity of deionized water obtained using our device at a controlled room temperature of 25°C with a solid line indicates the dynamic viscosity of the water taken from a reference [47].

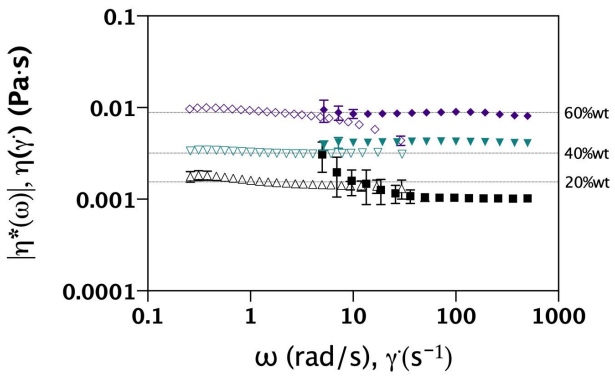

FIGURE 5. Modulus of the complex viscosities as a function of angular frequency (hollow symbols) obtained using our device, and shear-dependent viscosity (solid symbols) obtained by a rheometer (ARES G2, TA Instruments Inc.) of glycerol-water mixtures at the glycerol mass composition of 20%, 40%, and 60% at 25°C. The dashed lines were the measurement obtained from the literature [47].

device. In this measurement, the initial concentration of a glycerol solution was used as a solute since it has a very high viscosity of up to 945.0 mPa·s [47]. From this reason, the experiment was carried out to obtain the viscosity of the prepared glycerol-water mixtures, then, compared with the rheometer and reference value from a literature [47] as shown in Fig. 5.

According to Fig. 5, the obtained viscosity measurements using our device agreed with the reference viscosity from the literature [47]. The average absolute error of 20%wt, 40%wt, and 60%wt glycerol-water mixtures at 25°C were 2.27%, 1.80%, and 27.97% from the compact DDM, and 31.59%, 30.99%, and 2.87% from the reference rheometer. However, the measured viscosity at the angular frequency above 10.0 s^{-1} showed an unreliable result as it decreased upon an increase in the angular frequency. Unlike the result obtained using the rheometer, the obtained viscosity was inconsistent when compared with the reference values [47], particularly the glycerol content below 40%wt.

B. VALIDATION OF THE DeepDDM PLATFORM

The DeepDDM interpolates the image intensities by synthesizing in-between images of an original image series, producing different in-between motions of the embedded tracer particles in a measuring fluid. As a result, these additional images increase the frame rate of the original image series as its overall recording time is unchanged. However, validation is necessary for determining the rheological measurement accuracy of this approach compared with the rheometer measurement. In addition, this experiment is also aimed at discovering how many synthesized in-between images still yielded a reliable result. This can be done by repeating the procedure of the video frame interpolation algorithm to the previously synthesized image series. Then, the DDA was applied to the image series from no to the n in-between interpolations as shown in Fig. 6.

In this experiment, the 4,000 image series of the prepared artificial saliva was acquired by the DeepDDM at approximately 30.0 frames per second. In-between images were synthesized from the information of two adjacency images, producing a new image series from the FILM video interpolation. Then, the DDM analyzed the new image series to obtain the image structuring function. Following this, the

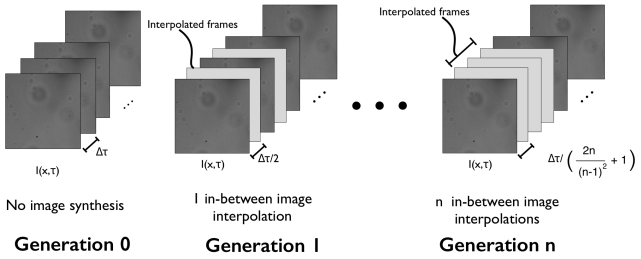

FIGURE 6. DeepDDM in-between image interpolation scheme.

average mean square displacement of the embedded tracer particles was determined as aforementioned. Accordingly, the Generalized Strokes-Einstein relation was applied to the mean square displacement yielding the corresponding viscoelastic modulus. The complex viscosity of the artificial saliva was determined from this modulus. The modulus of the obtained complex viscosity was used regarding the Cox-Merz relationship to compare with the shear viscosity obtained from the reference rheometer. However, this procedure was repeated with the previously interpolated image series up to generation four.

1) DEIONIZED WATER

Deionized water is a well-characterized fluid and usually used as a reference. In this experiment, viscosity of a deionized water was characterized using our DeepDDM with the video frame interpolation up to three generations and compared to those obtained from the published data at 0.89 $mPa \cdot s$ [47] as illustrated in Fig. 7.

From Fig. 7, the mean and standard deviation of the modulus of complex viscosity of deionized water measured at 25°C from 20-folded replications. The video frame interpolation generation 1 to 3 showed the mean and standard deviation of the viscosity were at 0.94± 0.01, 0.95± 0.02, and 0.93± 0.15 $mPa \cdot s$. When compared the measured viscosity to the reference, the average absolute error of the viscosity obtained from video frame interpolation of generation 1, 2, and 3 were 6.25%, 7.48%, and 9.16%, respectively. This might be caused by error propagation from each generation as the higher video frame generation generates new images based-on previous video frame generation. All things considered, the error was raised by the increment of the video frame interpolation generation. Although the error obtained from the video frame generation 1 shown the best accurate viscosity estimation, the angular frequency can be extended only two folded. Instead, the video frame interpolation of generation 2 yielded almost quadruple of the frequency while the viscosity estimation was in good agreement compared to the reference with less than 10% error. In additional, this error can be mitigated by implementing a temperature control of the sample for future improvements. From these reasons, we selected the video frame interpolation of generation 2 to artificial saliva on the next subsection.

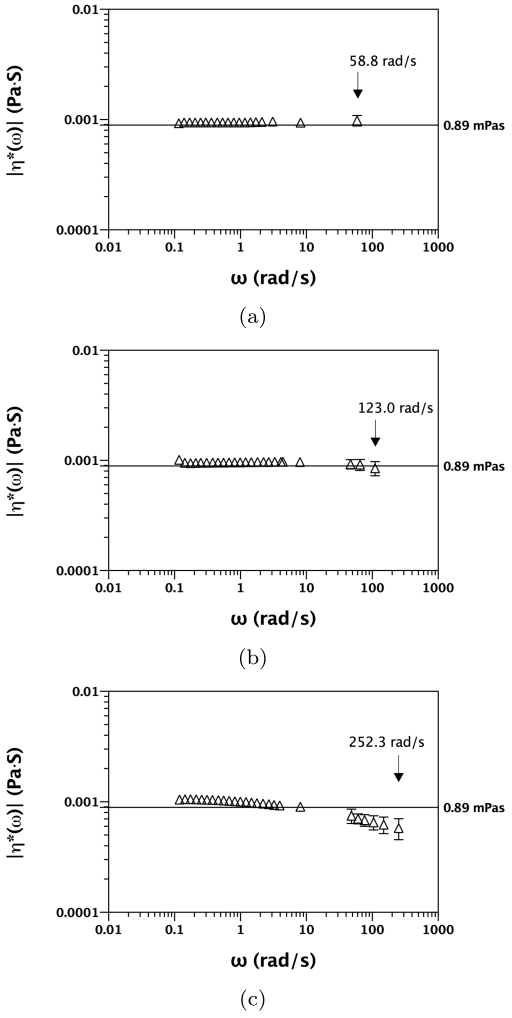

FIGURE 7. Modulus of complex viscosity of deionized water as a function of angular frequency measured at 25°C using our DeepDDM device of 20-folded replications. Figure 7(a), 7(b), and 7(c) represented the viscosity from video frame interpolation of generation 1, 2, and 3 respectively. The horizontal black solid lines indicated the viscosity of water obtained from [47].

2) ARTIFICIAL SALIVA

In this section, the experiment was carried out by measuring the initial concentration of the artificial saliva using the DeepDDM compared to the reference bulk rheometry.

a: BULK MEASUREMENT

An approximately 1.0 mL sample of the prepared artificial saliva was used to determine its viscosity using the reference rheometer. However, the temperature of the sample was controlled at 25°C before a measurement started. The steady-shear viscosity and torque of three-fold replication are shown in Fig. 8.

From Fig. 8, the steady-shear experiment of the artificial saliva showed unreliable viscosity measurement below the shear rate of 2.7 s^{-1} due to inconsistency of the torque. Thus, viscosity from the shear rate of 2.7 s^{-1} was used for comparison.

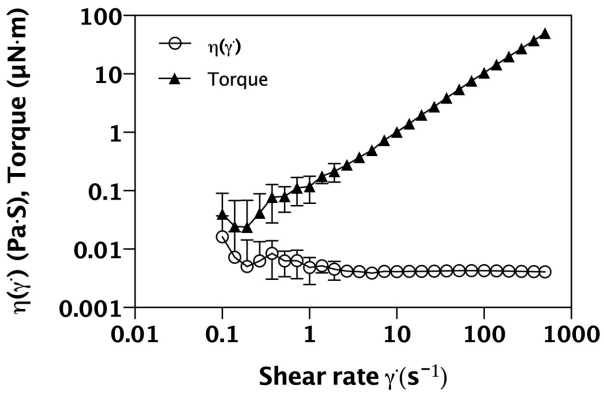

FIGURE 8. A steady-shear viscosity (Open circles) and torque (Solid triangles) plot of artificial saliva was obtained using the reference rheometer (ARES G2, TA Instruments Inc.)

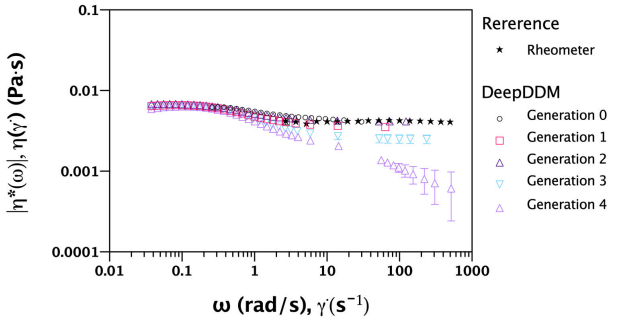

FIGURE 9. Modulus of the complex viscosity as a function of angular frequency (Hollow symbols) obtained using our DeepDDM device, and shear-dependent viscosity (Solid symbol) obtained using a rheometer (ARES G2, TA Instruments Inc.) of artificial saliva at 25°C. The solid symbols show the average modulus of the complex viscosity from generation zero to generation four. The error bars represent the standard deviation of the measurement from three-folded replication.

b: OUR DeepDDM RESULTS

In a measurement, approximately 8.0 μL of the artificial saliva was used for determining the modulus of complex viscosity in a controlled room temperature at 25°C. Our DeepDDM was carried out up to generation four in this experiment to estimate the complex viscosity of the artificial saliva. The measurement was three-fold replicated as shown in Fig. 9.

From Fig. 9, the result of one and two in-between frame interpolations agreed with the result obtained using the reference rheometer. In addition, the angular frequency of the original measurement from 30.1 rad/s was extended to a maximum of 63.5 and 123.0 rad/s in one and two in-between frame interpolations, respectively. In the angular frequency below 0.3 rad/s, the DeepDDM was also able to extend the measurement down to 0.04 rad/s. However, this angular frequency range was not validated due to the unreliable result in the frequency range obtained by the reference rheometer.

Nevertheless, the measured viscosity failed to achieve a valid result beyond three in-between image interpolations

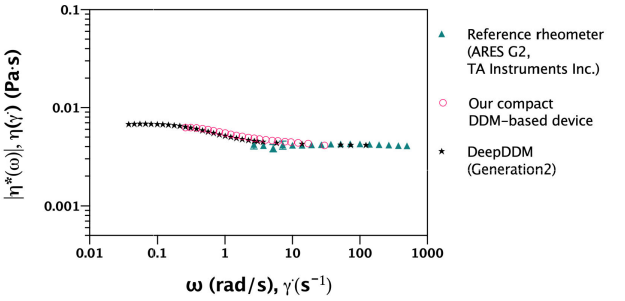

FIGURE 10. Modulus of the complex viscosity of an artificial saliva measured at 25°C. The solid black star represented the viscosity obtained from our DeepDDM device. The red circles showed the viscosity obtained by our compact DDM-based device. The upward green triangles illustrated the shear-dependent viscosity of the saliva obtained from the reference rheometer.

in the series (Generation 3). However, the one in-between image interpolation (Generation 2) produced the average absolute error at 5.45% when compared with the reference rheometer. In analogous to experiment with deionized water, the video frame interpolation of generation 2 achieved more comprehensive angular frequency than those obtained from generation one with acceptable error. Thus, the two in-between image interpolation was selected for our DeepDDM video frame interpolation. When compared with no in-between image (generation 0), our DeepDMM of the video frame generation 2 also yielded better accuracy with 7.85% compared to 13.47%.

To determine average absolute error of the measurements, these overlapped data were linearly interpolated to obtain identical frequencies (in x-axis). Following this, the interpolated data were compared against the viscosity obtained by the rheometer, resulting in the absolute error of 13.47% and 7.85% for the compact DDM and DeepDDM respectively. Therefore, the DeepDDM result extended the frequency ranges resulting in a more comprehensive frequency range of the measurement as illustrated in Fig. 10.

IV. DISCUSSIONS

We initially validated our compact differential dynamic microscopy-based device without the video frame interpolation algorithm considered as generation 0. Rheological measurements were carried out with two well-studied materials: deionized water and glycerol-water solutions. The viscosity obtained by the device was compared to the reference rheometer, including the published data [47].

According to the result, our compact DDM device can measure the fluid's viscosity below 3.2 $mPa \cdot s$, corresponding to 40%wt glycerol in water at 25 °C. On the contrary, the rheometer yielded a more reliable result at a higher viscosity of 60%wt glycerol in water at 25°C with the average absolute error of 2.87%. This is due to the fact that our device relied on passive micro-rheology in which there is no external force applied. Thus, measuring the motion of the employed tracer particles in a high-viscosity

fluid is quite challenging as this technique relies only on thermal motion, which can be difficult to generate sufficient deformation. However, this issue could be tackled by employing smaller tracer particles. Thus the particles more easily redistribute themselves according to the Stokes-Einstein relation. Nevertheless, the image resolution must be high so that the small employed particles are within the system's resolving power and become detectable. In contrast to our device, the rheometer can apply an external force to the probe for measuring a fluid's response, leading to a more reliable rheological characterization of a higher viscous fluid. Although the rheometer can measure much higher viscous fluid, it requires accurate mechanical motion control of the probe. The mechanical motion control is also quite limited to move the probe in micro-scale distance. For this reason, the rheometer may not obtain valid micro-scale rheological responses [55], particularly in a weak modulus fluid such as water at low shear rate.

In our DeepDDM device, the video interpolation at generation 2 was used for interpolating two in-between images, resulting in a quadruple of the measuring angular frequency in good agreement with the references. However, we also found that the different information in the interpolated data considerably fluctuated as an increment of interpolation generation. As a result, the average absolute error increased with the interpolation generation. This might be caused by error propagation from each generation. We could solve the problem by modifying the frame interpolation model to produce more in-between frames in one iteration instead of one image per iteration. Additionally, we can fine-tune the frame interpolation model, particularly for the particle movement images. Furthermore, our device measurement could be improved by additional temperature control of the sample. This is due to the fact that our device relies on thermal energy for measurement.

V. CONCLUSION

In this work, a compact deep-learning platform (DeepDDM) was developed for obtaining the micro-rheological of the fluid of interest. A quantitative rheological assessment of micro-volume fluid was carried out using this platform by exploiting the emerging technique of differential dynamic microscopy (DDM). The platform has two main components: a compact DDM-based device and a deep learning algorithm for in-between video frame interpolation. The device consisted of a few critical components fitted in a small 3D-printed housing, resulting in a compact and portable platform. Thus, the device can be performed at a local sample collection site, particularly for biological fluids, whose natural properties are usually changed over time [56]. For the measurement using our DeepDDM platform, a test fluid is filled with a tiny amount of tracer particles in an in-house micro-chamber accommodating approximately 8 μL of the fluid. As the particles undergo Brownian motion, the device records the tracer movement to a computer. The video frame interpolation based on a deep-learning algorithm was applied to the recorded data, producing a total of n-1 in-between images, where n is the total of the original image. These interpolated images, including the original images, were combined and referred to as a new image data set. Following this, the new image and the original data set were analyzed by the DDA yielding two image structuring functions. Then, these structure functions were merged according to the reference [52]. After which, a mean square displacement of such particles was obtained from the merged function. Then, the generalized Stokes-Einstein relation (GSER) was applied to retrieve the fluid's visco-elastic modulus. At this point, the complex viscosity of the fluid was obtained from this modulus. To compare with steady-shear viscosity, the modulus of the viscosity was calculated and plotted against the shear viscosity, referred to as the empirical Cox-Merz relationship. According to the experiment, the complex viscosity modulus obtained from our DeepDDM agreed with the steady-shear viscosity obtained using the reference rheometer up to two in-between frame interpolations. In comparison with no frame interpolation, the maximum accessible angular frequency range was extended from approximately 30.1 rad/s up to 123.0 rad/s. The result rheological responses of our DeepDDM were also in good agreement with a reference rheometer(ARES G2, TA Instrument) in a parallel plate setup with the average absolute error of the viscosity measurement were less than 10%. Thus our DeepDDM platform can produce a more comprehensive accessible angular frequency range than without in-between video frame interpolation applied.

REFERENCES

[1] T. Shinbrot, *Biomedical Fluid Dynamics: Flow and Form*. Oxford, U.K.: Oxford Univ. Press, 2019. [Online]. Available: https://books.google.co.th/books?id=aCiPDwAAQBAJ

[2] T. M. Squires and T. G. Mason, "Fluid mechanics of microrheology," *Annu. Rev. Fluid Mech.*, vol. 42, no. 1, pp. 413–438, Jan. 2010, doi: 10.1146/annurev-fluid-121108-145608.

[3] C. Yan and D. J. Pochan, "Rheological properties of peptide-based hydrogels for biomedical and other applications," *Chem. Soc. Rev.*, vol. 39, pp. 3528–3540, Sep. 2010, doi: 10.1039/B919449P.

[4] R. G. Schipper, E. Silletti, and M. H. Vingerhoeds, "Saliva as research material: Biochemical, physicochemical and practical aspects," *Arch. Oral Biol.*, vol. 52, no. 12, pp. 1114–1135, Dec. 2007.

[5] O. Manipon and M. Noe, "Effectiveness of chemicooking as a gamified intervention in nomenclature of compounds: Learning experiences of grade 11 students in a public school," *Int. Muldisciplinary Res. J.*, vol. 5, no. 1, Feb. 2023.

[6] S. P. Humphrey and R. T. Williamson, "A review of saliva: Normal composition, flow, and function," *J. Prosthetic Dentistry*, vol. 85, no. 2, pp. 162–169, Feb. 2001.

[7] W. H. Schwarz, "The rheology of saliva," *J. Dental Res.*, vol. 66, no. 2, pp. 660–666, Feb. 1987, doi: 10.1177/00220345870660S209.

[8] J. H. H. Bongaerts, D. Rossetti, and J. R. Stokes, "The lubricating properties of human whole saliva," *Tribology Lett.*, vol. 27, no. 3, pp. 277–287, Jul. 2007.

[9] S. J. Haward, J. A. Odell, M. Berry, and T. Hall, "Extensional rheology of human saliva," *Rheologica Acta*, vol. 50, nos. 11–12, pp. 869–879, Dec. 2011.

[10] M. N. Motoi, M. Lidia, and S. Swindells, "A device for the collection of submandibular saliva," *New Zealand dental J.*, vol. 108, no. 1, pp. 4–8, 2012.

[11] G. B. Proctor and G. H. Carpenter, "The function of salivary proteins and the regulation of their secretion by salivary glands," *Biomed. Rev.*, vol. 9, p. 3, Dec. 1998. [Online]. Available: https://journals.mu-varna.bg/index.php/bmr/article/view/132

[12] J. R. Stokes, M. W. Boehm, and S. K. Baier, "Oral processing, texture and mouthfeel: From rheology to tribology and beyond," *Current Opinion Colloid Interface Sci.*, vol. 18, no. 4, pp. 349–359, Aug. 2013.
[13] L. A. Tabak, "Structure and function of human salivary mucins," *Crit. Rev. Oral Biol. Med.*, vol. 1, no. 4, pp. 229–234, Oct. 1990, doi: 10.1177/10454411900010040201.
[14] J. Mathew, P. Sankar, and M. Varacallo, *Physiology, Blood Plasma*. StatPearls, FL, USA: StatPearls Publishing, 12023. [Online]. Available: https://www.ncbi.nlm.nih.gov/books/NBK531504/
[15] G. Késmárky, P. Kenyeres, M. Rábai, and K. Tóth, "Plasma viscosity: A forgotten variable," *Clin. Hemorheology Microcirculation*, vol. 39, no. 1–4, pp. 243–246, 2008.
[16] S. Jaiswal and P. K. Yadav, "A micropolar-newtonian blood flow model through a porous layered artery in the presence of a magnetic field," *Phys. Fluids*, vol. 31, no. 7, Jul. 2019, Art. no. 071901, doi: 10.1063/1.5100802.
[17] K. S. Breuer, *Microscale Diagnostic Techniques*. Cham, Switzerland: Springer, 2005.
[18] D. Weihs, T. G. Mason, and M. A. Teitell, "Bio-microrheology: A frontier in microrheology," *Biophysical J.*, vol. 91, no. 11, pp. 4296–4305, Dec. 2006.
[19] K. M. Schultz and E. M. Furst, "Microrheology of biomaterial hydrogelators," *Soft Matter*, vol. 8, no. 23, pp. 6198–6205, 2012, doi: 10.1039/C2SM25187F.
[20] E. Furst and T. Squires, *Microrheology*. Oxford, U.K.: Oxford Univ. Press, 2017. [Online]. Available: https://books.google.co.th/books?id=9xJIswEACAAJ
[21] R. H. Ewoldt, M. T. Johnston, and L. M. Caretta, *Experimental Challenges of Shear Rheology: How to Avoid Bad Data*. New York, NY, USA: Springer New York, 2015, pp. 207–241, doi: 10.1007/978-1-4939-2065-5_6.
[22] J. C. Lindon, G. E. Tranter, and D. W. Koppenaal, "Particle light scattering methods and applications," in *Encyclopedia of Spectroscopy and Spectrometry*, 3rd ed. Oxford, U.K: Academic Press, 2017, pp. 543–553.
[23] R. K. Tekade, "Importance of physicochemical characterization of nanoparticles in pharmaceutical product development," in *Basic Fundamentals of Drug Delivery* (Advances in Pharmaceutical Product Development and Research). New York, NY, USA: Academic Press, 2019, pp. 369–400.
[24] P. Worsfold, C. Poole, A. Townshend, and M. Mirâ, "Bioassays | enzyme assaysâ," in *Encyclopedia of Analytical Science*, 3rd ed. Oxford, U.K.: Academic Press, 2019, pp. 271–277.
[25] D. Some, "Light-scattering-based analysis of biomolecular interactions," *Biophysical Rev.*, vol. 5, pp. 147–158, 2013, doi: 10.1007/s12551-013-0107-1.
[26] B. Berne and R. Pecora, *Dynamic Light Scattering: With Applications to Chemistry, Biology, and Physics* (Dover Books on Physics). Mineola, NY, USA: Dover Publication, 2013. [Online]. Available: https://books.google.co.th/books?id=xg3CAgAAQBAJ
[27] P. C. Cai, B. A. Krajina, M. J. Kratochvil, L. Zou, A. Zhu, E. B. Burgener, P. L. Bollyky, C. E. Milla, M. J. Webber, A. J. Spakowitz, and S. C. Heilshorn, "Dynamic light scattering microrheology for soft and living materials," *Soft Matter*, vol. 17, no. 7, pp. 1929–1939, 2021, doi: 10.1039/D0SM01597K.
[28] S. Nimesh, "Tools and techniques for physico-chemical characterization of nanoparticles," in *Gene Therapy* (Woodhead Publishing Series in Biomedicine). Sawston, U.K.: Woodhead Publishing, 2013, pp. 43–63.
[29] E. H. Egelman, "Intrinsically disordered proteins," in *Comprehensive Biophysics*. Amsterdam, The Netherlands: Elsevier, 2012, pp. 170–211.
[30] T. G. Mason, "Estimating the viscoelastic moduli of complex fluids using the generalized stokes–einstein equation," *Rheologica Acta*, vol. 39, pp. 371–378, Aug. 2000, doi: 10.1007/s003970000094.
[31] T. G. Mason and D. A. Weitz, "Optical measurements of frequency-dependent linear viscoelastic moduli of complex fluids," *Phys. Rev. Lett.*, vol. 74, no. 7, pp. 1250–1253, Feb. 1995.
[32] R. Cerbino and V. Trappe, "Differential dynamic microscopy: Probing wave vector dependent dynamics with a microscope," *Phys. Rev. Lett.*, vol. 100, May 2008, Art. no. 188102.
[33] R. Cerbino and P. Cicuta, "Perspective: Differential dynamic microscopy extracts multi-scale activity in complex fluids and biological systems," *J. Chem. Phys.*, vol. 147, no. 11, Sep. 2017, Art. no. 110901, doi: 10.1063/1.5001027.
[34] J. Rička, "Dynamic light scattering with single-mode and multimode receivers," *Appl. Opt.*, vol. 32, no. 15, pp. 2860–2875, May 1993.
[35] L. Cipelletti and D. A. Weitz, "Ultralow-angle dynamic light scattering with a charge coupled device camera based multispeckle, multitau correlator," *Rev. Sci. Instrum.*, vol. 70, no. 8, pp. 3214–3221, Aug. 1999, doi: 10.1063/1.1149894.
[36] A. V. Bayles, T. M. Squires, and M. E. Helgeson, "Probe microrheology without particle tracking by differential dynamic microscopy," *Rheologica Acta*, vol. 56, no. 11, pp. 863–869, Nov. 2017, doi: 10.1007/s00397-017-1047-7.
[37] N. Willenbacher and C. Oelschlaeger, "Dynamics and structure of complex fluids from high frequency mechanical and optical rheometry," *Current Opinion Colloid Interface Sci.*, vol. 12, no. 1, pp. 43–49, Mar. 2007.
[38] G. Fritz, W. Pechhold, N. Willenbacher, and N. J. Wagner, "Characterizing complex fluids with high frequency rheology using torsional resonators at multiple frequencies," *J. Rheology*, vol. 47, no. 2, pp. 303–319, Mar. 2003, doi: 10.1122/1.1538608.
[39] B. Schroyen, D. Vlassopoulos, P. Van Puyvelde, and J. Vermant, "Bulk rheometry at high frequencies: A review of experimental approaches," *Rheologica Acta*, vol. 59, no. 1, pp. 1–22, Jan. 2020, doi: 10.1007/s00397-019-01172-w.
[40] M. Buchanan, M. Atakhorrami, J. F. Palierne, F. C. MacKintosh, and C. F. Schmidt, "High-frequency microrheology of wormlike micelles," *Phys. Rev. E, Stat. Phys. Plasmas Fluids Relat. Interdiscip. Top.*, vol. 72, no. 1, Jul. 2005, Art. no. 011504.
[41] J. S. Vesaratchanon, K. Takamura, and N. Willenbacher, "Surface characterization of functionalized latexes with different surface functionalities using rheometry and dynamic light scattering," *J. Colloid Interface Sci.*, vol. 345, no. 2, pp. 214–221, May 2010.
[42] A. S. M. Goh, B. S. Chuah, and K. C. Nguyen, *Rheological Properties of Personal Lubricants*. Tokyo, Japan: Springer, 2017, pp. 323–336, doi: 10.1007/978-4-431-56080-7_12.
[43] R. You and R. McGorty, "Two-color differential dynamic microscopy for capturing fast dynamics," *Rev. Sci. Instrum.*, vol. 92, no. 2, Feb. 2021, Art. no. 023702, doi: 10.1063/5.0039177.
[44] M. Arko and A. Petelin, "Cross-differential dynamic microscopy," *Soft Matter*, vol. 15, no. 13, pp. 2791–2797, 2019, doi: 10.1039/C9SM00121B.
[45] D. Mahajan, "Moving gradients: A path-based method for plausible image interpolation," *ACM Trans. Graph.*, vol. 28, no. 3, pp. 1–11, 2009.
[46] S. Meyer, O. Wang, H. Zimmer, M. Grosse, and A. Sorkine-Hornung, "Phase-based frame interpolation for video," in *Proc. IEEE Conf. Comput. Vis. Pattern Recognit. (CVPR)*, Jun. 2015, pp. 1410–1418.
[47] M. L. Sheely, "Glycerol viscosity tables," *Ind. Eng. Chem.*, vol. 24, no. 9, pp. 1060–1064, Sep. 1932, doi: 10.1021/ie50273a022.
[48] F. Giavazzi, D. Brogioli, V. Trappe, T. Bellini, and R. Cerbino, "Scattering information obtained by optical microscopy: Differential dynamic microscopy and beyond," *Phys. Rev. E Covering Statistical, Nonlinear, Biol., Soft Matter Phys.*, vol. 80, Sep. 2009, Art. no. 031403.
[49] L. G. Wilson, V. A. Martinez, J. Schwarz-Linek, J. Tailleur, G. Bryant, P. N. Pusey, and W. C. K. Poon, "Differential dynamic microscopy of bacterial motility," *Phys. Rev. Lett.*, vol. 106, no. 1, Jan. 2011, Art. no. 018101.
[50] M. A. Escobedo-Sánchez, J. P. Segovia-Gutiérrez, A. B. Zuccolotto-Bernez, J. Hansen, C. C. Marciniak, K. Sachowsky, F. Platten, and S. U. Egelhaaf, "Microliter viscometry using a bright-field microscope: η-DDM," *Soft Matter*, vol. 14, no. 34, pp. 7016–7025, 2018, doi: 10.1039/C8SM00784E.
[51] P. Edera, D. Bergamini, V. Trappe, F. Giavazzi, and R. Cerbino, "Differential dynamic microscopy microrheology of soft materials: A tracking-free determination of the frequency-dependent loss and storage moduli," *Phys. Rev. Mater.*, vol. 1, Dec. 2017, Art. no. 073804.
[52] D. Germain, M. Leocmach, and T. Gibaud, "Differential dynamic microscopy to characterize Brownian motion and bacteria motility," *Amer. J. Phys.*, vol. 84, no. 3, pp. 202–210, Mar. 2016, doi: 10.1119/1.4939516.
[53] F. Reda, J. Kontkanen, E. Tabellion, D. Sun, C. Pantofaru, and B. Curless, "Film: Frame interpolation for large motion," in *Computer Vision–ECCV*. Cham, Switzerland: Springer, 2022, pp. 250–266.
[54] T. Xue, B. Chen, J. Wu, D. Wei, and W. T. Freeman, "Video enhancement with task-oriented flow," *Int. J. Comput. Vis.*, vol. 127, no. 8, pp. 1106–1125, Aug. 2019.
[55] C. J. Pipe and G. H. McKinley, "Microfluidic rheometry," *Mech. Res. Commun.*, vol. 36, no. 1, pp. 110–120, 2009.
[56] C. Collett, A. Ardron, U. Bauer, G. Chapman, E. Chaudan, B. Hallmark, L. Pratt, M. D. Torres-Perez, and D. I. Wilson, "A portable extensional rheometer for measuring the viscoelasticity of pitcher plant and other sticky liquids in the field," *Plant Methods*, vol. 11, no. 1, p. 16, Mar. 2015, doi: 10.1186/s13007-015-0059-5.

UNGKARN JARUJAREET received the B.Eng. degree in computer engineering from Thammasat University, Thailand, the M.Eng. degree from Chulalongkorn University, Thailand, and the Ph.D. degree in biomedical engineering from the James Watt School of Engineering, University of Glasgow, U.K. He was appointed as a Researcher with the National Electronics and Computer Technology Center, Thailand. His current research interests include the micro-rheology of biological fluids, computer vision, and light scattering techniques.

KANNIKA WIRATCHAWA received the B.Sc. degree in statistical information from Khon Kaen University, Thailand, where she is currently pursuing the master's degree in applied statistics. Her current research interests include natural language processing, computer vision and pattern recognition, and machine learning.

PIYAPHONG PANPISUT received the Doctor of Dental Surgery (D.D.S.) degree from the Faculty of Dentistry, Thammasat University, Thailand, and the M.Sc. degree in conservative dentistry and the Ph.D. degree in biomaterials and tissue engineering from University College London. He is currently an Associate Professor of dental materials science with the Division of Restorative Dentistry, Faculty of Dentistry, Thammasat University. His current research interests include restorative dental materials, polymer-based materials, and biomaterials to prevent oral diseases.

THANAPONG INTHARAH received the B.Sc. degree in mathematics from Mahidol University, Thailand, the M.Sc. degree in computer science from Chulalongkorn University, Thailand, and the M.Sc. degree in machine learning and the Ph.D. degree in computer science from University College London, U.K., in 2018. He is currently an Assistant Professor of computer science with the Department of Statistics, Faculty of Science, Khon Kaen University, Thailand. His current research interests include the applications of computer vision and AI in healthcare. He is also working on AI-enhanced hardware, such as metering tools and smart glasses.